At what frequencies should air-core magnetics be used?

Michael Solomentsev, Alex J. Hanson

University of Texas at Austin
2501 Speedway, Austin, TX 78712, USA
mys432@utexas.edu, ajhanson@utexas.edu

***Abstract*—Magnetic components for power conversion (inductors and transformers) are often designed with magnetic cores, which add core loss but reduce the required number of turns, copper loss, and usually total loss. At very high frequencies, poor core materials make this tradeoff less advantageous and air-core magnetic components are often preferred. The boundary between the magnetic-core-preferred and air-core-preferred regimes has not yet been theoretically identified, and intermediate frequency ranges (e.g., 5 to 30 MHz) see both cored and air-core examples. In this work, we calculate various expressions that suggest that cored inductors can outperform their air-core counterparts up to many tens of MHz on a volumetric basis and about 10 MHz on a mass basis, based on the properties of currently available magnetic materials. We experimentally demonstrate the boundary frequencies by comparing the quality factors of optimized magnetic-core and air-core toroidal inductors. Formally demonstrating the advantage of magnetic-core over air-core inductors suggests more advantageous design strategies at tens of MHz, with significant impact on applications at industrial, scientific, and medical (ISM) frequency bands (6.78, 13.56, 27.12 MHz) and other rf frequencies.**

***Index Terms*—High Frequency (HF), Magnetics, Performance Factor, Core Loss, Copper Loss, Power Conversion**

I. Introduction

As power converters are more often being designed to operate using switching frequencies in the megahertz range, careful design of magnetic components is necessary to minimize losses, size, and/or weight. Typically, magnetic components are designed to have magnetic cores to reduce the number of turns required to achieve a target inductance and energy storage. The core does introduce core loss, but the tradeoff is usually advantageous at conventional power conversion frequencies (approximately 10 kHz to 1 MHz).

Both core and copper losses scale with frequency: the former due to micro- and macro-scopic eddy currents in the core, and the latter due to eddy currents in the windings. While skin depth decreases proportional to $f^{\frac{1}{2}}$ (and thus copper loss scales up at that rate), core loss is often modeled as proportional to f^{α} [1]–[3], where α is a material parameter with typical values between 1 and 2. Optimizing for loss at higher frequencies therefore requires more turns and larger gaps. For very high frequencies, it is both theoretically advantageous and practically convenient to design magnetic components with no core at all.

Air-core structures predominate in the 5 to 50 MHz space, across a variety of applications [4]–[8]. Converters are regularly designed to implement wireless power transfer for medical devices at the 6.78 MHz, 13.56 MHz, and occasionally 27.12 MHz. While this application space requires a coreless separation between the transmit and receive coils, many implementations at low frequency use magnetic back-plates while at MHz frequencies they often do not. In addition, matching networks are often necessary which usually rely on air-core inductors at MHz frequencies [9]–[13]. Moreover, high-frequency power inverters and their associated matching networks are used for plasma generation (necessary for semiconductor manufacturing), RF heating for food applications, and particle acceleration [14]–[16]. Such converters operate well into the tens of MHz and again predominantly use air-core magnetic components. Less application-oriented research has developed high-frequency resonant inverters that operate at 27.12 MHz [17], [18], 30 MHz [19], and up to 40.68MHz [20]. These examples all use air-core magnetics.

Designers may also have motivating factors besides total loss and volume when choosing between a magnetic or air core. Where EMI is a strong concern, magnetic-core inductors may be chosen to contain stray flux. In mass-sensitive applications, such as aerospace, air cores may be preferred.

A quantitative way to express the suitability of magnetic cores for operation at a particular frequency is with the performance factor $\mathcal{F} = \hat{B}f$, with units of mT·MHz. The performance factor is a material figure of merit that expresses the maximum B field $\hat{B}$ that can be imposed on a given material at a given frequency f before reaching a predefined core loss density (typically chosen between 200 and 500 mW/cm^3). It has been shown that the achievable power handling capability of a magnetic component is proportional to the performance factor or minor modifications to it [21]. Nevertheless, while the performance factor may be useful in comparing the relative suitability of core materials for operation across frequency, it does not directly provide a way to compare these materials to air. Nevertheless, it has been shown that several NiZn materials have good performance factors at tens of MHz [21], [22], suggesting that cored inductors may still be suitable for use at higher frequencies where air-core magnetics currently dominate.

This material is based upon work supported by the National Science Foundation under Grant No. DGE-1828974.

Some relatively recent examples of cored magnetics in the HF regime signal the potential for cored magnetics in this frequency domain. [23] uses a magnetic core for a 13.56 MHz ac inductor and achieves much higher quality factor (Q) than its air-core counterparts. [24] develops very high Q self-resonant magnetics for wireless power transfer at 6.78 MHz. These exceptions anecdotally suggest what this paper intends to formally demonstrate: that cored magnetics may be superior in many applications where air-core components are currently favored, depending on the main design constraints.

In this work, we calculate several expressions that represent the crossover point where air-core inductors theoretically outperform their cored counterparts in various situations. This work builds on the material presented in [25] adding performance factor data for additional materials to its survey, an analysis based on maintaining constant mass, and an analysis based on the necessary relative permeability. We conclude that components with magnetic cores maintain a volumetric advantage to many tens of MHz and a weight advantage to several MHz, with important implications for many of the applications listed above which today rely primarily on air-core components.

Section II begins by calculating the theoretical crossover point based on maintaining constant current density $\hat{J}$ and flux density $\hat{B}$ in air-core and magnetic-core inductors of equal volume. The result indicates the crossover point where air-core inductors outperform magnetic-core inductors occurs in the hundreds of MHz. Section III furthers this analysis by restricting the comparison to constant *total* power loss. This analysis suggests a crossover frequency of around 40 to 50 MHz compared to commercially-available materials. Section IV presents another independent analysis where total mass is held constant, finding a crossover point around 10 MHz. Section V presents an alternative derivation based on the minimum necessary permeability required for a magnetic material to outperform air.

In Section VI, we validate these expressions by designing magnetic-core and air-core inductors optimized for a certain volume/mass, target impedance, and frequency. Section VII presents a discussion of various non-idealities and limitations in our theoretical analysis. In Section VIII, we summarize our findings and note that there is significant potential for increased adoption of components with magnetic cores in the multi-MHz domain.

II. Theoretical Derivation Based on Constant $\hat{J}$ & $\hat{B}$

In this section and the next, we analyze a toroidal inductor with circular cross-section, whose labeled geometry is shown in Fig. 1. This structure is chosen as it effectively contains the flux whether a core is present or not, which makes for a more fair comparison. Nevertheless, the derivation is roughly valid for most classes of high-frequency inductors and transformers for power conversion, and the numerical results are strong enough that changing the geometry would most likely not suggest a different conclusion (see Section VII).

A. Derivation 1: Comparing Power Processing Capability

One potential method for identifying the threshold where air-core structures outperform cored structures is by comparing each of their power processing capabilities. We specifically consider sinusoidally-excited inductors with toroidal geometries and single-layer windings where the available conduction area is limited by the skin depth, shown in Fig. 1. Further assume that there are certain limitations on maximum loss densities, as has been done elsewhere [21], [26]. For an inductor with a magnetic core, these limits manifest themselves as a maximum peak AC flux density $\hat{B}$ based on a *core loss density limit* $P_{\mathrm{core,v}}$ and a maximum current density $\hat{J}$ based on a *copper loss density limit*, $P_{\mathrm{Cu,v}}$. The maximum voltage that can be applied to the component is given by Faraday's law and the flux density limit: $V = N\frac{d\phi}{dt} = NA_c\hat{B}\omega\cos\omega t$. Using the current density limit, $\hat{J}$, we calculate a peak current in the cored inductor, $I_{max} = \hat{J}\delta l_c/N$. This produces a maximum power handling capability for a cored inductor:

$$P_{cored} = \frac{1}{2}I_{max}V_{max} = \frac{1}{2}(NA_c\hat{B}\omega)\frac{\hat{J}\delta l_c}{N} = \frac{1}{2}A_c l_c \delta \hat{B}\hat{J}\omega \tag{1}$$

The above expression is calculated in [21] in the derivation of both the standard performance factor ($\mathcal{F} = \hat{B}f$) and modified performance factors. Note that a size-optimized component will always operate at its performance limit - i.e., if a component is not operating at $\hat{B}$, it can either be made smaller or it could process more power while staying within its budget.

In the case of an air-core inductor, voltage is not constrained by B field (because there is no core loss), but by inductance, $v = L\frac{di}{dt}$:

$$V = LI_{max}\omega = \frac{N^2}{\mathcal{R}}I\omega = \frac{N^2A_c\mu_0}{l_c}I\omega \tag{2}$$

The peak current for the air-core inductor is the same as in the magnetic-core case. We can therefore extract a maximum power handling capability for an air-core inductor:

$$P_{air-core} = \frac{1}{2}I_{max}V_{max} = \frac{N^2A_c\mu_0}{2l_c}(\frac{\hat{J}\delta l_c}{N})^2\omega = \frac{1}{2}\mu_0 A_c l_c \hat{J}^2\delta^2\omega = \frac{1}{\sigma}A_c l_c \hat{J}^2 \tag{3}$$

where σ represents the conductivity of copper and $\delta = \sqrt{\frac{2}{\omega\sigma\mu_0}}$ represents the skin depth. Comparing the power processing capability of both inductors yields:

$$\frac{P_{cored}}{P_{air-core}} = \frac{\frac{1}{2}A_c l_c\delta\sigma\hat{B}\hat{J}\omega}{A_c l_c \hat{J}^2} = \frac{\delta\sigma\hat{B}\omega}{2\hat{J}} = \frac{\pi\delta\sigma\mathcal{F}}{\hat{J}} \tag{4}$$

where $\mathcal{F} = \hat{B}f$ is the conventional performance factor. When the above expression is equal to 1, the power processing capabilities of two equivalently-sized magnetic-core & air-core inductors are equal, given the same loss density constraints. Thus, (4) can be used to identify a threshold to distinguish

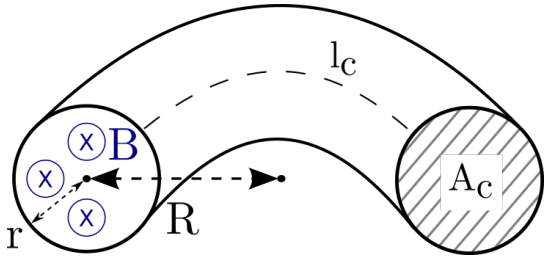

Fig. 1: Labeled geometry of a toroid with a circular cross-section, showing its cross-sectional radius, r, and its radius of revolution, R.

when it is more advantageous to use a core:

$$1 \leq \frac{\pi\delta\sigma\mathcal{F}}{\hat{J}} = \frac{\pi\sigma\mathcal{F}}{\hat{J}}\sqrt{\frac{2}{\omega\sigma\mu_0}} = \frac{\pi\mathcal{F}\sqrt{\sigma}}{\hat{J}\sqrt{\frac{1}{2}\omega\mu_0}} = \frac{\pi\mathcal{F}}{\frac{1}{2}\sqrt{P_{\mathrm{Cu,v}}\omega\mu_0}} \tag{5}$$

$$\mathcal{F} \geq \sqrt{\frac{\mu_0 f P_{\mathrm{Cu,v}}}{\pi}} \tag{6}$$

Evaluating whether (6) is true is easily done on a graph of performance factor versus frequency. When (6) is true, this calculation suggests that magnetic-core components will be volumetrically superior to air-core components. Further analysis is provided in Section II-C.

B. Derivation 2: When Required l_g Equals l_c

This same expression can be calculated through an alternate method. Consider the design of a magnetic-core inductor with an air gap. When using a core with sufficiently high permeability, inductance will be almost entirely determined by the length of the air gap (as opposed to the length of the core). As frequency increases, the required gap length to maintain constant core loss density in the core increases as well (since the allowed B field, $\hat{B}$, decreases with frequency). The cross-over point where air-core components are more advantageous (for a given volume) occurs when the calculated gap length, l_g, reaches total core length, l_c. We begin by establishing a target inductance:

$$L = \frac{N^2}{\mathcal{R}} = \frac{N^2\mu_0 A_c}{l_g} = \frac{N^2\mu_0 A_c}{l_c} \tag{7}$$

where we have set $l_g = l_c$, which is true at the boundary where air-core magnetics become more volumetrically advantageous. Just as before, the inductor has limits on maximum B field and current density, set by loss density requirements. These limitations will constrain the turn count and current: $N = l_g\hat{B}/\mu_0 I$ (which again holds when $l_g = l_c$). Then we substitute this requirement into the expression for inductance:

$$L = \frac{\mu_0 A_c l_g^2 \hat{B}^2}{\mu_0^2 l_g I^2} = \frac{A_c l_g \hat{B}^2}{\mu_0 I^2} = \frac{A_c l_g (\hat{B} f)^2}{\mu_0 f^2 I^2} = \frac{A_c l_g \mathcal{F}^2}{\mu_0 f^2 I^2} \tag{8}$$

After moving the inductance over to the right hand side of the expression, it can be further simplified by noting that N^2 is proportional to inductance, and eliminating the remaining geometric quantities. Converting to an inequality and isolating performance factor produces the same result as the derivation presented in Section II-A.

$$1 \leq \frac{A_c l_g \mathcal{F}^2}{\mu_0 L f^2 \frac{\hat{J}\delta l_g}{N}^2} = \frac{\pi\sigma A_c \mathcal{F}^2}{l_g f \hat{J}^2}\frac{N^2\mathcal{R}}{N^2} = \frac{\pi\sigma A_c \mathcal{F}^2}{l_g f \hat{J}^2}\frac{l_g}{\mu_0 A_c} \tag{9}$$

$$\mathcal{F} \geq \sqrt{\frac{\mu_0 f \hat{J}^2}{\pi\sigma}} = \sqrt{\frac{\mu_0 f P_{\mathrm{Cu,v}}}{\pi}} \tag{10}$$

C. Analysis

Equation (6) expresses the performance factor threshold which distinguishes whether a cored component will outperform an air-core component. That threshold is a function of a maximum allowable copper loss density $P_{\mathrm{Cu,v}}$. If we assume the allowable copper loss density for the air-core structure is the same as that of a magnetic-core inductor, e.g. $P_{\mathrm{Cu,v}} = 200$ mW/cm^3, the expression yields $\mathcal{F} = .282\sqrt{f}$, where f is in MHz and $\mathcal{F}$ is in mT·MHz. For frequencies at which data is available, material performance factors sit well above this constraint (see the black dashed curve plotted in Fig. 2). Projecting out a trend line based on the existing envelope of performance factors suggests an intersection in the hundreds of MHz.

While the calculated result is dependent on the choice of $P_{\mathrm{Cu,v}}$, the square-root dependence is weak and the resulting performance factor value is very small. As a result, the qualitative conclusion and the estimate of crossover frequency remain strong regardless of the particular value of $P_{\mathrm{Cu,v}}$ chosen.

III. Theoretical Derivation Based on Constant Total Loss

A. Derivation

The previous section's analysis followed from assumptions that core and copper loss densities should be held constant. It may be more advantageous to consider alternative constraints, as using a constant value for copper loss density may unfairly penalize air-core structures. It could reasonably be argued that, since air-core structures have no core loss, their allowable copper loss density could be higher than in their magnetic-core counterparts. As such, we consider an alternative derivation based on constant *total* loss.

Let us begin by assuming equal distribution of total loss between core and copper in the cored case. This is often roughly true - it is well understood that optimized designs will not be dominated by core nor copper loss [29], but the exact balance may vary depending on the particular design. To make the analysis tractable, we will assume that core loss and copper loss are equal for magnetic-core inductors.

$$P_{diss} = P_{\mathrm{Cu,cored}} + P_{\mathrm{Core,cored}} = 2P_{\mathrm{Core,cored}} = 2A_c l_c P_{\mathrm{core,V}} \tag{11}$$

With this restriction in mind, we calculate the power processing capability of the magnetic-core inductor, just as was done in Section II. The restriction on $\hat{B}$ and thus voltage still applies

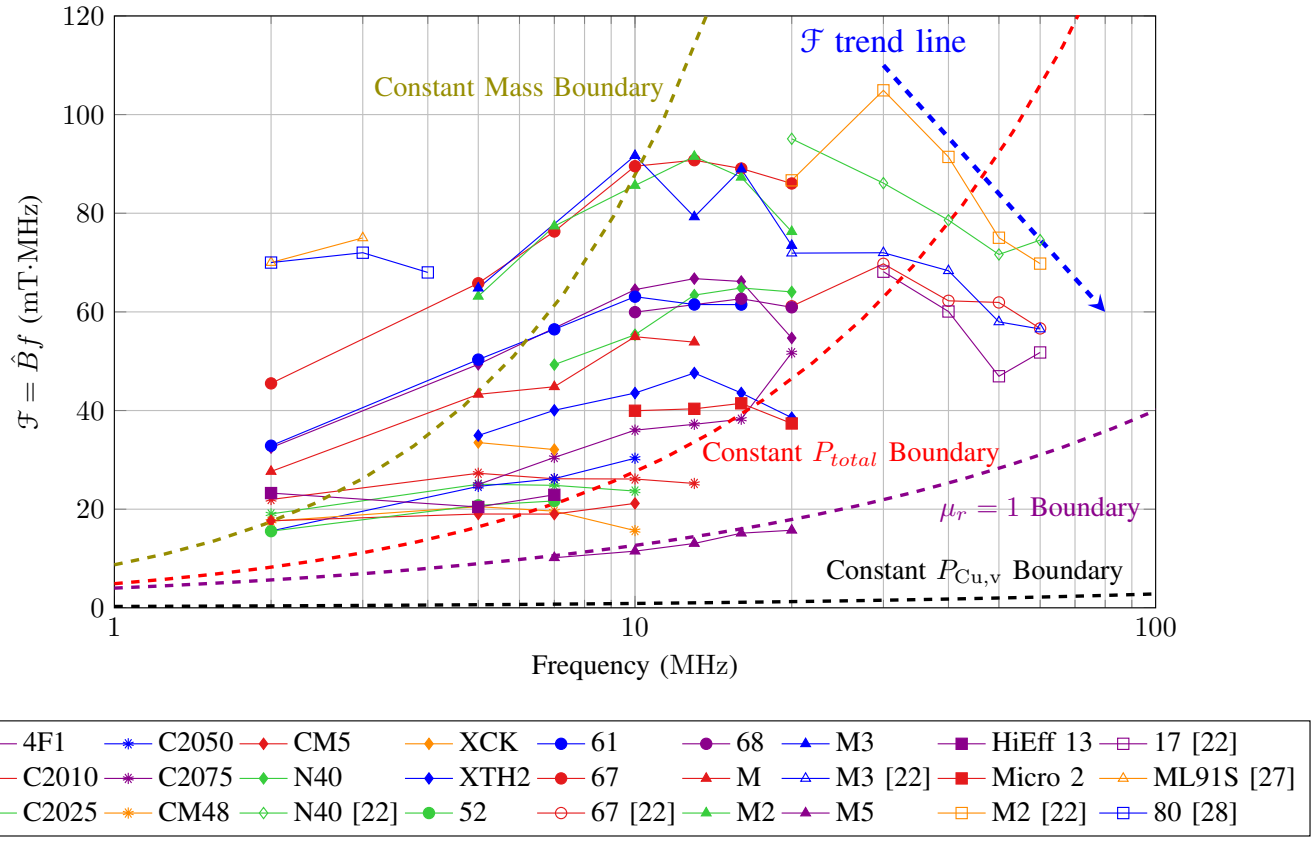

Fig. 2: Survey of $\mathcal{F}$ [21]. Dashed lines show the envelope of performance factor as frequency increases (in blue) and the calculated crossover point for $P_V = 200$ mW/cm^3 and cross-sectional radius of 5 mm for the various derived expressions: Constant $P_{\mathrm{Cu,v}}$ in black, constant P_{total} in red, constant mass in orange, and $\mu_r = 1$ in purple.

($V_{max} = NA_c\hat{B}\omega$). However, the current is now restricted by a limit on maximum copper loss:

$$P_{\mathrm{Cu,cored}} = \frac{1}{2}I_{max}^2 R = I_{max}^2 \frac{1}{2}\frac{2\pi r N}{\delta\sigma^{l_c}/_N} \tag{12}$$

Note that we consider a toroid with a circular cross-section, as shown in Fig. 1, with with cross-sectional radius r and radius of revolution R. Thus, $A_c = \pi r^2$ and $l_c = 2\pi R$. The maximum allowed current is therefore:

$$I_{max} = \sqrt{\frac{\delta\sigma l_c P_{\mathrm{Cu,cored}}}{\pi r N^2}} = \sqrt{\frac{\delta\sigma A_c l_c^2 P_{\mathrm{core,V}}}{\pi r N^2}} \tag{13}$$

We can combine the maximum voltage and current expressions to find the total power processing capability of the magnetic-core inductor:

$$P_{cored} = \frac{1}{2}I_{max}V_{max} = \frac{1}{2}A_c l_c \hat{B}\omega\sqrt{\frac{\delta\sigma A_c P_{\mathrm{core,V}}}{\pi r}} \tag{14}$$

We would like to compare (14) to the power handling capability of an air-core component. In this analysis, we choose to hold the *total* loss budget constant – the air-core component is therefore allowed to have higher copper loss. Since total power dissipation is held constant and we previously assumed that core loss and copper loss should be equal for a magnetic-core component, we can conclude for an air-core component that $P_{\mathrm{Cu,air}} = 2P_{\mathrm{Cu,cored}}$, and thus:

$$I_{max} = \sqrt{\frac{2\delta\sigma A_c l_c^2 P_{\mathrm{core,V}}}{\pi r N^2}} \tag{15}$$

The maximum voltage can be related to the maximum current ($V = LI\omega$), and an expression for the total power processing capability of the air-core structure can be produced:

$$P_{air-core} = \frac{1}{2}L\omega I_{max}^2 = \frac{1}{2}\frac{N^2 A_c \mu_0 \omega}{l_c}\frac{2\delta\sigma A_c l_c^2 P_{\mathrm{core,V}}}{\pi r N^2} = \frac{1}{\pi r}A_c^2 l_c \delta\sigma\mu_0\omega P_{\mathrm{core,V}} \tag{16}$$

The ratio of power processing capability under the constant-total-loss constraint can then be derived:

$$\frac{P_{cored}}{P_{air-core}} = \frac{\pi r\hat{B}}{2A_c\delta\sigma\mu_0 P_{\mathrm{core,V}}}\sqrt{\frac{\delta\sigma A_c P_{\mathrm{core,V}}}{\pi r}} = \frac{\hat{B}}{2\mu_0\sqrt{r\delta\sigma P_{\mathrm{core,V}}}} = \frac{\hat{B}f^{1/4}\pi^{1/4}}{2\mu_0^{3/4}\sigma^{1/4}r^{1/2}P_{\mathrm{core,V}}^{1/2}} \tag{17}$$

Which can be translated into a new performance factor threshold:

$$\mathcal{F} \geq \frac{2}{\pi^{1/4}}\mu_0^{3/4}\sigma^{1/4}r^{1/2}P_{\mathrm{core,V}}^{1/2} = 2\sqrt{rP_{\mathrm{core,V}}\sqrt{\frac{\mu_0^3\sigma}{\pi}}} \tag{18}$$

Again, material performance factors above this threshold suggest that a magnetic-core component will volumetrically out-perform an air-core component at that frequency.

B. Analysis

For a P_v of 200 mW/cm^3 and a r of 5 mm, the core/air-core threshold comes out to: $\mathcal{F} = 4.9 f^{\frac{3}{4}}$ (where f is in MHz and $\mathcal{F}$ is in mT·MHz). This threshold is plotted on Fig. 2 in red.

Figure 2 shows a selection of performance factors of magnetic materials designed for high-frequency operation. Note that while the envelope of the commercially available performance factor decays with frequency, many materials sit higher than both of the thresholds calculated so far – one assuming fixed loss densities and the other assuming a fixed total loss budget. This is true well into the tens of MHz. Based on the envelope of best performing materials, the crossover point where air-cores begin to out-perform magnetic-core inductors appears to be approximately 40 to 50 MHz when total loss is constrained, as opposed to the estimate of hundreds of MHz when $\hat{B}$ and $\hat{J}$ were individually constrained. Many published designs in the 5-50 MHz space use air-core components, but this analysis suggests that cored structures would reduce loss further in the same volume, as in [23], [30]. Cored structures may also reduce the fields exterior to the magnetic structure, reducing EMI, loss, and the need for shielding [31].

IV. Theoretical Derivation Based on Constant Mass

A. Derivation

In many applications (biomedical, aerospace, etc.) component weight is a critical concern [32]. As such, it may be of interest to identify the crossover point given a constant mass requirement. We proceed by putting the power processing limits derived in Section II-A in terms of a constant mass, M, and core and copper mass densities, ρ_{core} and ρ_{cu} respectively (note that ρ is reserved for mass densities in this paper and we therefore refer only to the conductivity σ of copper rather than its resistivity).

$$P_{cored} = \frac{1}{2} A_c l_c \delta \hat{B} \hat{J} \omega = \frac{1}{2} \frac{M}{\rho_{core}} \delta \hat{B} \hat{J} \omega \tag{19}$$

where we have assumed that the magnetic-core component's weight is dominated by the core itself. For a toroid with a circular cross-section, $VOL_{core} = (\pi r^2)(2\pi R)$ and $VOL_{cu} = \delta(2\pi r)(2\pi R)$, assuming that the entire surface area of the toroid will be used for conduction. This produces a ratio of: $VOL_{core}/VOL_{cu} = (r/2\delta)$, which is utilized below.

$$P_{air-core} = \rho A_c l_c \hat{J}^2 = \rho (\frac{r}{2\delta} Vol_{Cu}) \hat{J}^2 = \rho \hat{J}^2 \frac{r}{2\delta} \frac{M}{\rho_{Cu}} \tag{20}$$

Comparing the power processing capability of both inductors yields:

$$\frac{P_{cored}}{P_{air-core}} = \frac{\frac{1}{2}\delta \hat{B} \hat{J} \omega \frac{M}{\rho_{core}}}{\rho \hat{J}^2 \frac{r}{2\delta} \frac{M}{\rho_{Cu}}} = \frac{\delta^2 \hat{B} \omega}{\rho \hat{J} r} \frac{\rho_{Cu}}{\rho_{core}} \tag{21}$$

Which can be rewritten as an inequality in terms of $\mathcal{F}$:

$$\mathcal{F} \geq \frac{1}{2} f \mu_0 \hat{J} r \frac{\rho_{core}}{\rho_{Cu}} \tag{22}$$

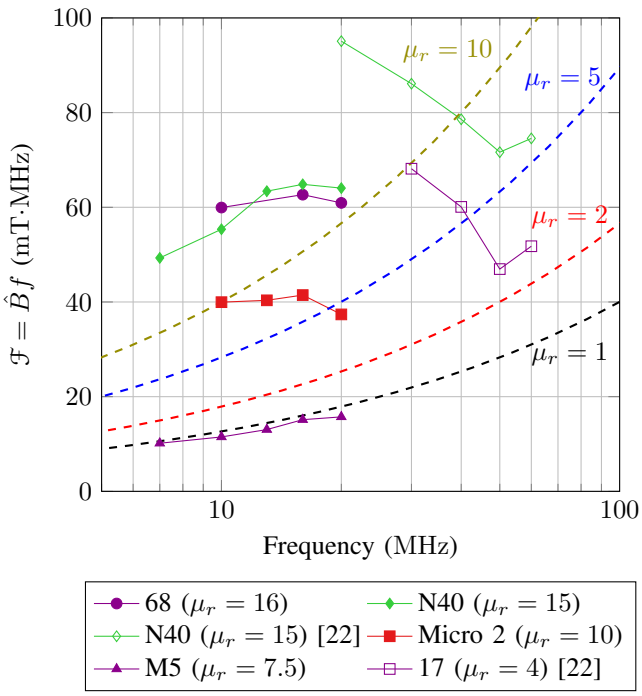

Fig. 3: $\mathcal{F}$ of materials with low permeability ($4 < \mu_r < 16$), plotted against several boundaries showing theoretical limits for un-gapped inductor performance (for $P_{\text{core,v}} = 200$ mW/cm^3 and $Q = 100$

A performance factor higher than this threshold at a particular frequency would indicate that a magnetic-core inductor would process more power than its air-core counterpart for the same mass and loss densities.

B. Analysis

When evaluated for typical values ($\rho_{core} = 5$ g/cm^3; $\hat{J} = 500$ A/cm^2; $r = 5$ mm), (21) yields $\mathcal{F} = 8.73 f$ (where f is in MHz and $\mathcal{F}$ is in mT·MHz). This threshold is plotted on Fig. 2 in orange. This expression predicts that air-core components will be able to process more power per unit mass than magnetic-core components beyond 10 MHz. For magnetic-core inductors to compete at these elevated frequencies would require materials with much lower density or with extremely high performance factors (orders of magnitude better than those of today's commercially-available materials). However, this analysis does indicate that there exist some materials (Fair-Rite 67, National Magnetics Group M3) that can be used to build magnetic-core inductors which outperform their equivalent-mass air-core counterparts to about 10 MHz, and that there are several more (the aforementioned, Fair-Rite 80, Hitachi Metals ML91S, Ferroxcube 4F1) that can do so up to about 5 MHz.

V. Theoretical Derivation Based on Required Permeability

A. Derivation

Another approach to examine the suitability of materials for high-frequency operation is through the lens of permeability.

We analyze a situation where permeability is a limiting factor for performance, akin to what is presented in [33].

Consider an inductor with a peak B field, $\hat{B} = \frac{LI}{NA_c}$, set by some loss density budget. For a given core, a target $\hat{B}$ and L can be reached simultaneously by varying the number of turns and the gap length. As the permeability of the core material decreases (all else equal), L would be maintained by decreasing l_g. The component's performance would be unchanged. If permeability were decreased too far, however, the required gap length l_g would be less than 0 and it would no longer be possible to meet the inductance and B-field requirements simultaneously.

There is therefore a critical permeability $\mu_{r,crit}$ above which the component's theoretical performance is constant, but below which the component will be sub-optimal. This critical permeability will be a function of the material loss characteristics and target application requirements. If the performance factor of available materials is low enough to cause $\mu_{r,crit}$ to fall below 1, this may be taken as an indication that air-core components are preferable at the frequency of interest.

As such, consider the case where permeability is indeed a limiting factor, and no gap is inserted into the structure. The target inductance sets a specific value for N, which can be substituted into the expression for $\hat{B}$ (to simplify the expression, we begin with $\hat{B}^2$):

$$\hat{B}^2 = \frac{L^2 I^2}{\frac{l_c}{\mu_r \mu_0 A_c} A_c^2} = \frac{\mu_r \mu_0 L I^2}{l_c A_c} = \frac{\mu_r \mu_0 E_{store}}{1/2\ Vol_{core}} \tag{23}$$

where E_{store} represents the energy stored in the inductor ($\frac{1}{2}LI^2$). Note that $\hat{B}$ can be related to performance factor, $\mathcal{F}$, and that Q is related to ratio of energy stored to energy lost in the structure, $2\pi E_{store}/E_{loss}$:

$$\mathcal{F}^2 = \frac{\mu_r \mu_0 f^2 Q E_{loss}}{\pi V O L_{core}} \tag{24}$$

Finally, we can express core loss density in terms of the remaining quantities. If core and copper loss are approximately equal (often true in many optimized designs), then $P_{\text{core,v}} \approx \frac{E_{loss} f}{2 Vol_{core}}$. The following expression is obtained:

$$\mathcal{F} = \sqrt{\frac{2\mu_r \mu_0 Q f P_{\text{core,v}}}{\pi}} \tag{25}$$

As long as performance factors larger than (25) exist, then this derivation suggests that the use of a core with permeability greater than μ_r will overall be advantageous. In particular, if μ_r is set to 1, then (25) can be used to see if available magnetic materials can outperform air.

B. Analysis

We propose three potentially useful interpretations of (25), which is plotted against experimental data from low-permeability magnetic materials in Fig. 3. It is helpful to recall that the energy stored in the core material is $\frac{1}{2\mu_0\mu_r}\hat{B}^2 \times Vol_{core}$.

- A material falling above the threshold indicates that it can be used in an un-gapped inductor that meets the specified performance requirements. In other words, the core material itself can store enough energy $\propto \hat{B}^2 \propto \mathcal{F}^2$ to meet the application requirements. While inserting a gap is trivial in many E- & pot-cores, it may be physically difficult (as seen in Section VI) and add manufacturing cost for toroidal structures. However, utilizing an un-gapped structure means that a designer loses one of their free parameters (along with N), and may not be able to maximally utilize their loss budget while meeting a target inductance.
- For even moderately high permeabilities, the expression yields extremely high values for the performance factor threshold, far above those of available materials in the high-frequency regime. This simply means that gaps must be inserted into these inductors to meet the design targets, which grants a second degree of freedom in design. This indicates that lower permeabilities could just as easily meet design constraints. It makes sense that lower permeability lowers the derived threshold, because low permeability increases the energy that can be stored in the core — $\propto 1/\mu_r$ for a given limit on B field.
- As real performance factors approach the limit defined by $\mu_r = 1$, (25) yields yet another theoretical threshold for the suitability of cored magnetics, plotted on Fig. 2 in purple. For a material at this limit, adding a gap no longer enables any control over inductance or B, as the permeability of the core is now equal to that of air. As such, falling below this threshold indicates that a magnetic material is too lossy to achieve the design constraints, and an air core would be preferable.

VI. Experimental Verification

A. Constant Volume Tests

To validate (6) and (18), several pairs of cored and air-core high-frequency inductors were built. Each pair was designed to have the same volume, operating frequency, average power loss density, and target impedance. We used toroidal cores as outlined in our analysis above. Each inductor was optimized for high performance in order to make the comparison fair. The optimization process is described in greater detail in Appendix A.

Based on the performance factors shown in Figure 2, a magnetic material best suited for each operating frequency was chosen (i.e. the materials with the highest performance factors at each frequency): Fair-Rite 67 for 10 MHz; National

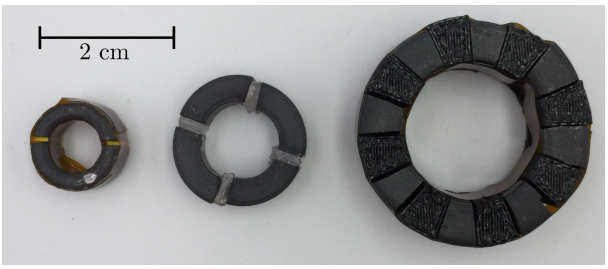

Fig. 4: Unwound toroidal cores showing implementation of quasi-distributed gaps for 10, 30, and 60 MHz.

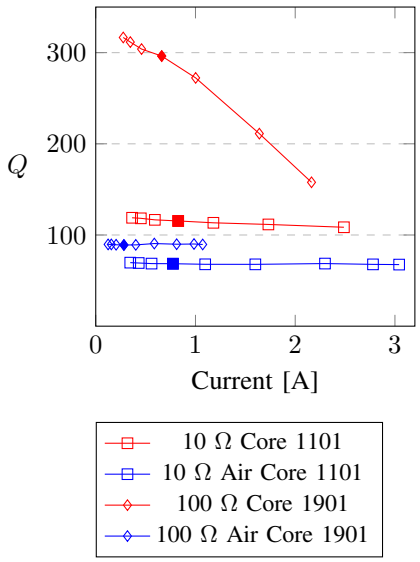

(a) Optimized Fair-Rite 67 and air-core inductors operating at 10 MHz

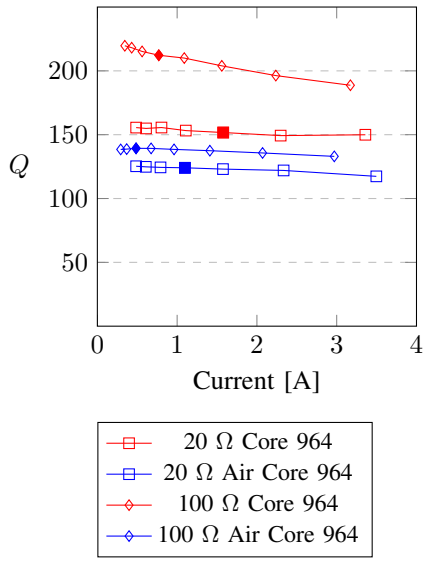

(b) Optimized M2 and air-core inductors operating at 30 MHz

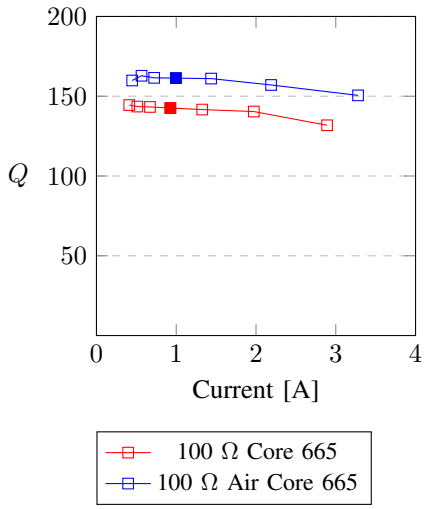

(c) Optimized N40 and air-core inductors operating at 60 MHz

Fig. 5: Experimental Q measurements from the constant volume test plotted against peak sinusoidal drive current at various frequencies, showing substantially higher performance from cored inductors at 10 and 30 MHz compared to their constant volume air-core counterparts. Each dataset is labeled with its impedance and part number (or part number of its equivalently sized core, in the case of the air-core data). The filled in data points correspond to approximately $P_v = 200$ mW/cm^3.

Magnetics Group M2 for 30 MHz; and NMG N40 for 60 MHz (note that NMG M3 has a *slightly* higher performance factor than Fair-Rite 67 at 10 MHz, but the latter material was used because it was readily available). Single frequency operation and full utilization of core surface area using foil windings (or standard magnet wire, depending on the turn count and toroid size) were assumed. By calculating copper and core loss for each case, optimized core designs were produced for an average total loss density of 200 mW/cm^3. This process produced optimized designs specifying how much of each core should be removed (i.e., how much of the toroid should be magnetic material, versus air), ensuring constant volume between core and air-core tests.

While the percentage of core to total volume was high in the 10 MHz case (91% to 98%, depending on the core), it was significantly smaller in the 30 MHz (75% to 86%) and 60 MHz (45% to 56%) cases. This required the use of quasi-distributed gaps [34] to minimize fringing flux and ensure the accuracy of the optimization. Intact toroids were sliced into smaller pieces using a 3400 RPM diamond lapidary saw, then taped or glued together with appropriately sized gaps. Figure 4 shows a selection of cores across different frequencies: the 67 core has two gaps, the M2 core has four, and the N40 core is constructed from eight pieces of a core sliced into 16ths, then assembled using a 3D printed jig. Using the volume of the magnetic-core toroid as a fixed target in each case, a similar optimization script for air-core structures was run. These air-core toroids were built as toroids with circular cross-sections, as opposed to the rectangular cross-sections of the cores shown in Fig. 4. Unconstrained by core dimensions, we varied both the toroid's cross-sectional radius and its axial radius while keeping total cylindrical volume constant, varying turn count to achieve target impedance. This again led us to an optimized design for a particular power loss density in each case. These specifications were used to create 3D print non-magnetic "cores" for the air-core toroids. The experimental impedances for both the core and air-core inductors are shown in Table I, which shows strong matching between each pair.

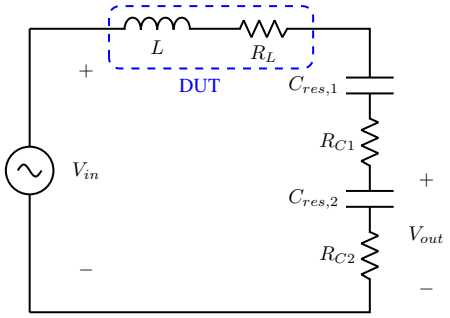

Fig. 6: Schematic of the inductor quality factor measurement setup.

The quality factor of the inductors was then measured using a series resonant testing setup, shown in Fig. 6. Such an approach has been used to characterize magnetic materials and high quality factor inductors [21]–[23], [35]. The method works by resonating the inductor under test with a capacitance. At the resonant frequency, the ratio between V_{out} and V_{in} is ideally directly proportional to the quality factor of the tested inductor. For high quality factor structures or high frequency measurements, it may be necessary to use a capacitor divider as shown to mitigate the effect of probe capacitance and otherwise account for losses not in the DUT (this was done for the tests described here). A full derivation of the quality

factor expression is performed in [35].

$$Q = \frac{\omega L}{\frac{V_{in}}{V_{out}}\sqrt{R_{C2}^2 + \frac{1}{\omega C_{res,2}^2}^2} - R_{C1} - R_{C2}} \tag{26}$$

Each inductor was tested at its operating frequency and a variety of drive currents, corresponding to various power loss densities. Small-signal quality factors for the air-core inductors were also collected using an E5061B impedance analyzer (with 3 GHz bandwidth) to validate the testing rig; the results match well with our experimental measurements, which indicates that the series resonant approach was valid.

The results are shown in Figure 5. In both the 10 and 30 MHz cases, core materials significantly outperform their air-core counterparts, by factors of roughly 3.5 and 1.7 respectively for the 100 Ω inductors. At 60 MHz, where (18) indicates that an air-core inductor should outperform an N40 toroidal inductor, experimental data indicates the air-core structure had roughly 20% larger Q than the cored inductor. These results show strong agreement with the predicted total loss based threshold, (18).

We note that the 60 MHz core had an extremely large air gap which required repeated core slicing to produce many still-large air gaps. These cuts needed to be sanded down, and the resulting structure is not exactly 43% core, as our optimization process specified. Moreover, both the 60 MHz cored and air-core inductors utilized 17 AWG round magnet wire, not foil. Repeated experimentation with foil and round windings found that round wire designs routinely outperformed foil-wound designs, despite the ostensibly smaller conduction area. This is due to current crowding at the thin edges of foil windings, for which we present a more thorough justification in Appendix B. Considering that the presented analysis assumes even distribution of current over the toroid surface, this could have been a significant factor in lowering the measured quality factors. Further discussion of the practical limitations of the analysis are presented in Section VII.

The cored inductor's superiority at 10 and 30 MHz and its competitiveness with the air-core version at 60 MHz, a frequency at which cored magnetics are rarely used, further indicates the potential of cored structures in high frequency applications.

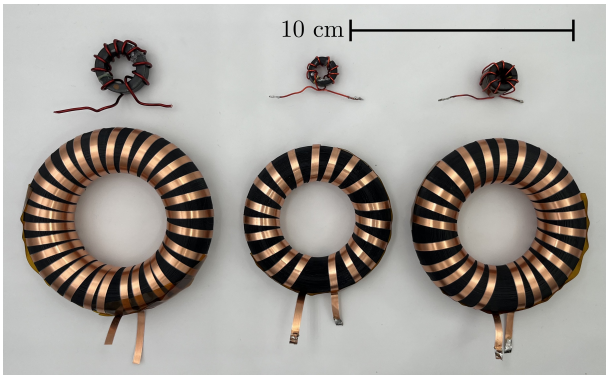

Fig. 7: Mass equivalent cored and air-core inductor pairs optimized for 1, 5, and 10 MHz (from left to right).

B. *Constant Mass Tests*

A second set of tests were conducted to validate (21). Cored inductors were optimized and built in the same process described in Section VI-A. Fair-Rite 80 was used at 1 MHz, and Fair-Rite 67 at 5 and 10 MHz. The theoretical mass of these designs was calculated by weighing the core and adding the theoretical copper volume, based on full coverage of core surface area and skin depth thickness. Air-core counterparts were again designed, this time holding their mass constant (again, assuming full coverage of surface area with one skin depth thickness). The optimized designs had their cores 3-D printed and wound. Fig. 7 shows the constant-mass inductor pairs - note the substantially larger volume (∼100x) of the air-core structures over the cored structures. The experimentally achieved impedances and masses are shown in Table I.

The quality factor of the inductors was measured using the same series-resonant testing rig as used in the constant volume tests. The experimental Q measurements are shown in Fig. 8. For all three cases, the cored structures outperform their air-core counterparts by significant margins. The filled-in data points on Fig. 8 correspond to a loss density of 200 mW/cm^3. In each case, the cored inductor is able to process more power (higher current) for the same loss density, indicating the validity of Equation (21).

Fig. 7 shows that the air-core toroids were wound with foil windings, not wire, despite the potentially higher performance of wire-wound designs (see Appendix B). For this particular test, it was critical for our prototypes to have constant mass. That constant mass value was calculated based on an assumption of utilizing the full surface area of the toroid for conduction. As such, foil was used to wind the air-core designs (foil narrow enough to wind the cored designs was not available, and copper composed a much smaller portion of their total mass). To verify that this was not a significant contributor to the final results, a wire version of the 25 Ω 5 MHz inductor was wound: It had approximately 20% higher Q than its foil version, but weighed 9.53 g instead of 2.29 g (∼3x the cored mass). It was still outperformed by the cored design. Building toroids that do match the full assumptions about conductor distribution would likely require unconventional strategies like 3D printing or deposition [36].

VII. Limitations & Discussion

The derivations presented in sections II, II-A, IV, and V rely on a variety of simplifications and assumptions, primarily to make the analysis tractable. There are several factors which may lead to deviations from the crossover points predicted in this work.

1) Toroid Cross-sectional Geometry: As shown in Fig. 1, the presented analysis assumes toroids have circular cross-sections. While this was the case for the air-core toroids manufactured for Section VI, most commercially available toroidal magnetic cores, including those used in this work, have rectangular cross-sections. While we only present analysis for the circular case, one can calculate corresponding

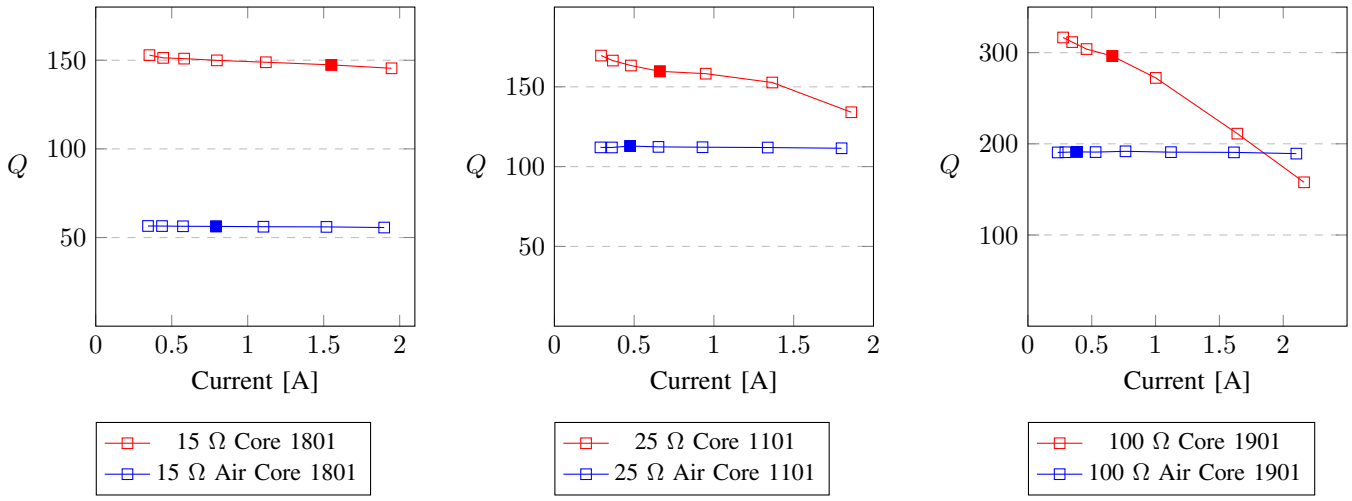

(a) Optimized Fair-Rite 80 and air-core inductors operating at 1 MHz

(b) Optimized Fair-Rite 67 and air-core inductors operating at 5 MHz

(c) Optimized Fair-Rite 67 and air-core inductors operating at 10 MHz

Fig. 8: Experimental Q measurements from the constant mass experiment plotted against peak sinusoidal drive current at various frequencies, showing substantially higher performance from cored inductors at 1, 5, and 10 MHz. Each dataset is labeled with its impedance and part number (or part number of the core in its equivalent mass counterpart, in the case of the air-core data). The filled in data points correspond to approximately $P_v = 200$ mW/cm^3 for the magnetic-core inductors and $P_{\mathrm{Cu,v}} = 200$ mW/cm^3 for the air-core inductors.

Constant Volume Tests					
Target Z [Ω]	F [MHz]	Material	Volume [cm^3]	Core Z [Ω] (L [nH])	Air-Core Z [Ω] (L [nH])
10	10	67	.49	13.2 (211)	13.1 (210)
100	10	67	.99	103.6 (1650)	101.6 (1617)
20	30	M2	1.31	20.3 (108)	20.1 (107)
100	30	M2	1.31	113.7 (603)	114.8 (609)
100	60	N40	4.83	110.8 (294)	103.3 (274)

Constant Mass Tests							
Target Z [Ω]	F [MHz]	Material	Target Mass [g]	Core Z [Ω] (L [nH])	Core Mass [g]	Air Z [Ω] (L [nH])	Air Mass [g]
15	1	80	7.23	15.6 (2480)	9.79	13.7 (2180)	4.3
25	5	67	2.11	25.7 (817)	2.89	26.1 (830.5)	2.29
100	10	67	4.06	103.7 (1650)	5.01	105.9 (1686)	3.44

TABLE I: Target and realized impedance data for the core and air-core experimental inductors, showing good agreement with target values and between inductor pairs.

expressions for the rectangular case. For example, for the constant mass analysis, we utilize a ratio between core & copper volumes ($r/2\delta$): For a rectangular toroid with inner diameter d, outer diameter D, and thickness T, this ratio is: $Vol_{core}/Vol_{cu} = T(D^2 - d^2)/(2\delta(D^2 - d^2 + 2TD + 2Td))$. For a toroid with a square cross-section (i.e., $T = .5(D - D)$), this simplifies to $Vol_{core}/Vol_{cu} = T/4\delta$. This is almost equivalent to the calculated expression, considering that the T term in this expression is the width of the core cross-section, i.e. $2r$ in the circular case. This suggests that while specific geometries may have specific versions of (18) and (21) that could improve the accuracy of our predictions, these variations are unlikely to be large in magnitude.

2) Non-sinusoidal Waveforms & DC Bias: This work primarily uses the standard Steinmetz equation ($P_v = kf^{\alpha}\hat{B}^{\beta}$, or $P_v = k\hat{B}^{\beta}$ at a particular frequency). While generally effective for purely sinusoidal waveforms, there are several factors which limit the applicability of the Steinmetz equation. Magnetics in power converters are often subject to non-sinusoidal current waveforms, such as square or triangular waves, with significant high frequency harmonics. Due to the nonlinear nature of core loss, calculating loss in these cases is not as simple as summing the loss for each component of the frequency spectrum. Rather, alternative approaches have been developed to accurately predict loss in these cases [1]–[3], all of which are more complicated than the simple Steinmetz equation used in this work. Moreover, a DC bias (again regular in many power converter applications) can also cause core losses to be higher than expected. This phenomenon is neither well understood nor captured by theoretical core loss modeling approaches. These factors may cause core losses to be higher than our theoretical calculations predict, lowering the real-world crossover frequency in these cases. Our experimental data, collected using pure sinusoidal currents, does match our theoretical predictions.

3) Flux Distribution: While the analysis assumed uniform

flux distribution throughout the core, this is a simplification. Flux does not travel uniformly throughout core pieces, and instead tends to crowd towards paths of lowest reluctance. In toroidal core pieces, this effect manifests in flux concentrating close to the inner radius of the toroid, while in E/I, pot, and planar cores flux tends to concentrate near corners. This effect can also cause theoretical underestimation of core losses, and thus potentially an overestimation of the theoretical cross-over frequency. This effect is likely to be greater in cores where flux concentrates around sharp corners (like E/I cores) and less significant in the toroids used in this work.

4) Current Crowding: It is well-understood that at high frequencies, current tends to crowd toward regions of high H-field. In toroidal inductors, that H-field is supposed to be contained within the toroid itself, inevitably, flux leaks from the main magnetic path and causes current crowding on the sides of conductors. This leads to the experimentally observed higher performance of round wires over foil windings described in Section VI and examined in Appendix B. More generally, this phenomenon does violate the outlined assumptions of the presented analysis, specifically the assumption of even conduction over the surface area of the toroid. This affects both cored and air-core magnetics, but since copper loss is the only component of loss for air-core magnetics, this would likely push real-world crossover frequencies higher.

5) Dimensional Scaling: While Fig. 2 shows calculated boundaries for only one value of cross-sectional radius (5 mm), equations (18) and (21) are somewhat sensitive to this parameter. Varying cross-sectional radius from 1 to 10 mm changes the projected frequency at which commercially available materials fall below the boundary from approximately 80 MHz (projecting out a trend-line for $\mathcal{F}$) to around 35 MHz for the constant total power loss expression and from 60 MHz to 6 MHz for the constant mass expression. Nevertheless, even the lower bounds for the cross-over frequencies suggest that cored inductors could be used at much higher frequencies than what is typical. If the cored inductors tested in Section VI had circular cross-sections, their effective cross-sectional radii would range from 2.2 to 4.4 mm (with the 60 MHz toroid being the largest). This suggests that if smaller toroids made from high-performing magnetic materials were to be tested, it may be possible to have cored inductors outperform air-cores even in the 60 to 80 MHz range.

6) Loss Density Scaling: Fig. 2 presents performance factors based on a loss density of 200 mW/cm^3, corresponding to the values for P_v used in the derived expressions. It is possible to use alternative values for the P_v limit, but the performance factor values must be scaled as well (this is not entirely straightforward, and requires knowledge of β for each material/frequency pair). Fig. 9 shows the envelope of highest performance factors at 500 mW/cm^3, along with the appropriately scaled thresholds. The two calculated thresholds that do intersect the envelope do so at roughly similar frequencies as in Fig. 2 (a few MHz higher for the constant mass and constant total power loss boundaries).

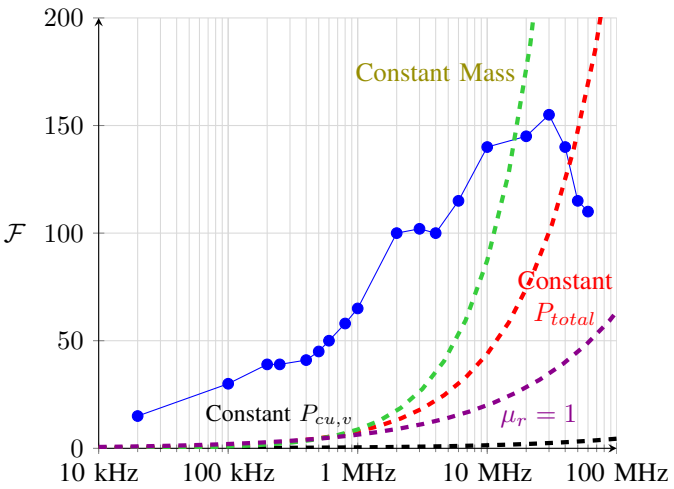

Fig. 9: The performance factor envelope of commercially available materials plotted against the derived thresholds in this paper: Constant $P_{cu,V}$ in black; constant P_{total} in red; constant mass in green; $\mu_r = 1$ in purple (all for $P_V = 500$mW/cm^3 and $r = 5$ mm).

VIII. Conclusion

While high frequency power converters typically rely on air-core magnetic components to avoid disproportionately large core loss, the region of validity of this design choice is not well understood, potentially leaving available performance on the table in applications operating at frequencies of about 5-50 MHz. In this work, we derive several formal expressions that indicate the frequency at which air-core magnetic components supersede their cored counterparts for a given volume or for a given mass. This boundary depends largely on the performance factor of the magnetic cores in question. The envelope of best-performing commercially available magnetic materials is plotted against the derived thresholds in Fig. 9. Based on the performance factors of commercially available magnetic cores, air-core inductors only eclipse cored inductors well into the VHF regime at around 50 MHz on a volumetric basis, and around 10 MHz on a mass basis (depending on the exact size of the magnetics used). We validate this conclusion by building a series of cored and air-core inductors optimized at 10, 30, and 60 MHz with identical impedance and volume. By measuring the quality factor of these inductors, we show agreement with our theoretical derivation and show higher performance of cored structures in the 10s of MHz. We do the same for several inductor pairs built with constant mass, and verify higher performance up to 10 MHz. Importantly, magnetics designed for these frequencies almost always feature air cores, indicating significant potential for improved performance by adopting magnetic materials in these applications.

Appendix A
Inductor Optimization Strategy

As described in Section VI, optimized inductors were built to test the validity of the analysis. Magnetic materials were chosen based on their performance factors at the frequencies

of interest (1, 5, 10, 30, and 60 MHz). Commercially available toroidal cores were purchased and their dimensions were run through an optimization script, as described below, and shown in the presented flowchart.

Given the dimensions of a commercially available magnetic core, the magnetic material's properties, operating frequency, and target inductance, an optimized inductor design was created. Following the analysis presented in Section II-B, the 'percent core' of the inductor was swept - this method of changing the gap guaranteed constant volume. For each option, turn count was calculated to reach target inductance. Turns were assumed to be foil turns that fully utilized the surface area of the toroid for conduction. A drive current was selected arbitrarily, core & copper losses were then calculated for each option. The option with minimum loss was then checked for its estimated loss density. Our analysis used a figure of 200 mW/cm^3, so we targeted this figure for the optimized loss density. If the selected candidate design's P_V was far from 200 mW/cm^3, a new current was chosen and the process was repeated until an optimized inductor with the correct loss density was produced. Note, however, that the final result was relatively insensitive to drive current, often only shifting by a few percent (in core material composition ratio) depending on what drive current was selected.

Once magnetic cored inductors were designed, the process was repeated with air-core inductors. For each cored inductor, an air-core counterpart with identical volume or mass (depending on the test), operating frequency, and inductance was built. The optimization process was largely similar, except because only volume (and not toroid dimensions) was fixed, the shape of the toroid could be varied. A variety of target candidates were generated by sweeping outer & inner diameters of a cylindrical toroid while holding volume constant. Again, in each case the number of turns was calculated to reach the target inductance, and were treated as perfectly distributed foil conductors. The same optimization point was ran from this point on, and the optimized design was then 3D printed, wound, and tested.

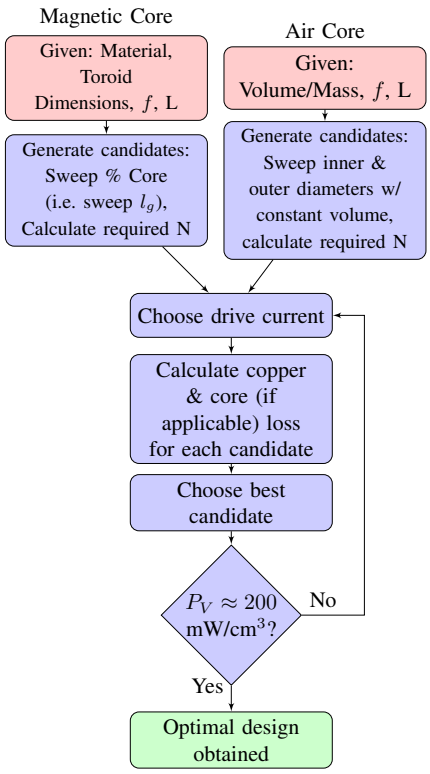

Appendix B
Choice of Foil vs. Round Windings

The analysis presented in Appendix A assumes full utilization of toroid surface area by the use of foil windings. However, the final tested inductors used in this article utilized traditional round wires (using either the largest wire gauge geometrically possible or readily available). This may seem like a willful sacrifice of performance for winding convenience, but that is not the case. When tested, inductors wound with round wire regularly outperformed their foil wound counterparts with the same core and number of turns. We aim to briefly explain this phenomenon and justify this design choice.

It is well understood that the main issues of concern for conduction at high frequencies are the skin and proximity effects, which, if not planned for, can cause copper losses to balloon. A foil winding aims to mitigate these effects by presenting a long and flat cross-section (ostensibly with a thickness greater than a skin depth at the target operating frequency) for current to conduct. However, if current does not flow on the long axis of the foil winding, but instead crowds on its edges, loss can be significantly greater than expected. We posit that within a toroidal inductor, proximity effects cause exactly this phenomenon to occur.

Figure 10 shows two finite element simulations of toroidal inductors with identical cores and number of turns. Despite lower utilization of core surface area, the wire wound case has peak current density and total copper loss 59.1% and 30.3% lower than its foil wound counterpart, respectively. This indicates that even in cases where proximity effects are often ignored, like that of the foil winding around an inductor, current crowding due to them can significantly increase loss. As such, all of our inductors utilized round wire windings to minimize loss and maximize Q.

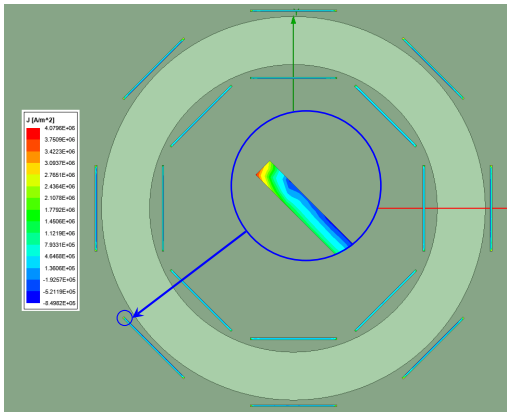

(a) FEA Simulation of foil wound inductor.

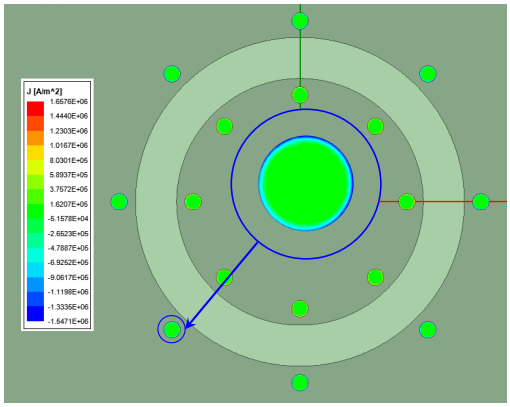

(b) FEA Simulation of traditional wire wound inductor.

Fig. 10: FEA Simulations of two identical inductors with varying winding styles. Note the lower peak current density in the round wire case.

REFERENCES

[1] J. Reinert, A. Brockmeyer, and R. De Doncker, "Calculation of losses in ferro- and ferrimagnetic materials based on the modified steinmetz equation," *IEEE Transactions on Industry Applications*, vol. 37, no. 4, pp. 1055–1061, 2001.

[2] K. Venkatachalam, C. Sullivan, T. Abdallah, and H. Tacca, "Accurate prediction of ferrite core loss with nonsinusoidal waveforms using only steinmetz parameters," in *2002 IEEE Workshop on Computers in Power Electronics, 2002. Proceedings.*, 2002, pp. 36–41.

[3] J. Muhlethaler, J. Biela, J. W. Kolar, and A. Ecklebe, "Improved core-loss calculation for magnetic components employed in power electronic systems," *IEEE Transactions on Power Electronics*, vol. 27, no. 2, pp. 964–973, 2012.

[4] G. Zulauf and J. M. Rivas-Davila, "Single-turn air-core coils for high-frequency inductive wireless power transfer," *IEEE Transactions on Power Electronics*, vol. 35, no. 3, pp. 2917–2932, 2020.

[5] P. Hazucha, G. Schrom, J. Hahn, B. Bloechel, P. Hack, G. Dermer, S. Narendra, D. Gardner, T. Karnik, V. De, and S. Borkar, "A 233-mhz 80four-phase dc-dc converter utilizing air-core inductors on package," *IEEE Journal of Solid-State Circuits*, vol. 40, no. 4, pp. 838–845, 2005.

[6] C. R. Sullivan, W. Li, S. Prabhakaran, and S. Lu, "Design and fabrication of low-loss toroidal air-core inductors," in *2007 IEEE Power Electronics Specialists Conference*, 2007, pp. 1754–1759.

[7] C. D. Meyer, S. S. Bedair, B. C. Morgan, and D. P. Arnold, "High-inductance-density, air-core, power inductors, and transformers designed for operation at 100–500 mhz," *IEEE Transactions on Magnetics*, vol. 46, no. 6, pp. 2236–2239, 2010.

[8] C. R. Sullivan, D. V. Harburg, J. Qiu, C. G. Levey, and D. Yao, "Integrating magnetics for on-chip power: A perspective," *IEEE Transactions on Power Electronics*, vol. 28, no. 9, pp. 4342–4353, 2013.

[9] S. Sinha, A. Kumar, S. Pervaiz, B. Regensburger, and K. K. Afridi, "Design of efficient matching networks for capacitive wireless power transfer systems," in *2016 IEEE 17th Workshop on Control and Modeling for Power Electronics (COMPEL)*, 2016, pp. 1–7.

[10] S. Liu, M. Liu, S. Yang, C. Ma, and X. Zhu, "A novel design methodology for high-efficiency current-mode and voltage-mode class-e power amplifiers in wireless power transfer systems," *IEEE Transactions on Power Electronics*, vol. 32, no. 6, pp. 4514–4523, 2017.

[11] Y. Lu and W.-H. Ki, "A 13.56 mhz cmos active rectifier with switched-offset and compensated biasing for biomedical wireless power transfer systems," *IEEE Transactions on Biomedical Circuits and Systems*, vol. 8, no. 3, pp. 334–344, 2014.

[12] T. C. Beh, M. Kato, T. Imura, S. Oh, and Y. Hori, "Automated impedance matching system for robust wireless power transfer via magnetic resonance coupling," *IEEE Transactions on Industrial Electronics*, vol. 60, no. 9, pp. 3689–3698, 2013.

[13] S. Aldhaher, D. C. Yates, and P. D. Mitcheson, "Design and development of a class ef_2 inverter and rectifier for multimegahertz wireless power transfer systems," *IEEE Transactions on Power Electronics*, vol. 31, no. 12, pp. 8138–8150, 2016.

[14] P. Piyasena, C. Dussault, T. Koutchma, H. S. Ramaswamy, and G. B. Awuah, "Radio frequency heating of foods: Principles, applications and related properties—a review," *Critical Reviews in Food Science and Nutrition*, vol. 43, no. 6, pp. 587–606, 2003, pMID: 14669879. [Online]. Available: https://doi.org/10.1080/10408690390251129

[15] S. Sinha, Y. Hou, D. Ni, Q. Ji, A. Persaud, P. Seidl, T. Schenkel, A. Lal, and K. K. Afridi, "A 27.12-mhz 10-kv power amplifier for compact particle accelerators utilizing an optimized matching network," in *2020 IEEE Energy Conversion Congress and Exposition (ECCE)*, 2020, pp. 5452–5457.

[16] S. Aldhaher, D. C. Yates, and P. D. Mitcheson, "Modeling and analysis of class ef and class e/f inverters with series-tuned resonant networks," *IEEE Transactions on Power Electronics*, vol. 31, no. 5, pp. 3415–3430, 2016.

[17] L. Raymond, W. Liang, J. Choi, and J. Rivas, "27.12 mhz large voltage gain resonant converter with low voltage stress," in *2013 IEEE Energy Conversion Congress and Exposition*, 2013, pp. 1814–1821.

[18] L. Roslaniec, A. S. Jurkov, A. A. Bastami, and D. J. Perreault, "Design of single-switch inverters for variable resistance/load modulation operation," *IEEE Transactions on Power Electronics*, vol. 30, no. 6, pp. 3200–3214, 2015.

[19] J. M. Rivas, Y. Han, O. Leitermann, A. D. Sagneri, and D. J. Perreault, "A high-frequency resonant inverter topology with low-voltage stress," *IEEE Transactions on Power Electronics*, vol. 23, no. 4, pp. 1759–1771, 2008.

[20] A. Clements, V. Vishnoi, S. Dehghani, and T. Johnson, "A comparison of gan class e inverter and synchronous rectifier designs for 13.56 mhz, 27.12 mhz and 40.68 mhz ism bands," in *2018 IEEE Wireless Power Transfer Conference (WPTC)*, 2018, pp. 1–4.

[21] A. J. Hanson, J. A. Belk, S. Lim, C. R. Sullivan, and D. J. Perreault, "Measurements and performance factor comparisons of magnetic materials at high frequency," *IEEE Transactions on Power Electronics*, vol. 31, no. 11, pp. 7909–7925, 2016.

[22] Y. Han, G. Cheung, A. Li, C. R. Sullivan, and D. J. Perreault, "Evaluation of magnetic materials for very high frequency applications," *IEEE Transactions on Power Electronics*, pp. 425–435, 2008.

[23] R. S. Bayliss III, R. S. Yang, A. J. Hanson, C. R. Sullivan, and D. J. Perreault, "Design, implementation, and evaluation of high-efficiency high-power radio-frequency inductors," in *2021 IEEE Applied Power Electronics Conference and Exposition (APEC)*, 2021.

[24] A. L. F. Stein, P. A. Kyaw, and C. R. Sullivan, "Wireless power transfer utilizing a high-q self-resonant structure," *IEEE Transactions on Power Electronics*, vol. 34, no. 7, pp. 6722–6735, 2019.

[25] M. Solomentsev and A. J. Hanson, "At what frequencies should air-core magnetics be used?" in *2022 IEEE Applied Power Electronics Conference and Exposition (APEC)*, 2022, pp. 625–632.

[26] C. R. Sullivan, B. A. Reese, A. L. F. Stein, and P. A. Kyaw, "On size and magnetics: Why small efficient power inductors are rare," in *2016 International Symposium on 3D Power Electronics Integration and Manufacturing (3D-PEIM)*, 2016, pp. 1–23.

[27] *Mn-Zn soft ferrite cores for high frequency power supplies MaDC-F*, Hitachi Metals Ltd., 2019. [Online]. Available: http://www.hitachi-metals.co.jp/e/products/catalog/sm/madc-f.pdf

[28] *80 Material Data Sheet*, Fair-Rite Products Corp., 2013. [Online]. Available: https://www.fair-rite.com/80-material-data-sheet/

[29] Erickson, Robert W. and Dragan Maksimović, *Fundamentals of Power Electronics*. Springer, 2001.

[30] D. W. Lee, K.-P. Hwang, and S. X. Wang, "Fabrication and analysis of high-performance integrated solenoid inductor with magnetic core," *IEEE Transactions on Magnetics*, vol. 44, no. 11, pp. 4089–4095, 2008.
[31] D. J. Perreault, C. R. Sullivan, R. S. Yang, R. Bayliss, and A. J. Hanson, "Self-shielded high frequency inductor," United States Application Patent 63/150,704, 2021.
[32] J. Zou, N. C. Brooks, S. Coday, N. M. Ellis, and R. C. Pilawa-Podgurski, "On the size and weight of passive components: Scaling trends for high-density power converter designs," in *2022 IEEE 23rd Workshop on Control and Modeling for Power Electronics (COMPEL)*, 2022, pp. 1–7.
[33] A. Hanson, "Opportunities in magnetic materials for high-frequency power conversion," *MRS Communications*, Aug. 2022. [Online]. Available: https://doi.org/10.1557/s43579-022-00225-1
[34] J. Hu and C. Sullivan, "Ac resistance of planar power inductors and the quasidistributed gap technique," *IEEE Transactions on Power Electronics*, vol. 16, no. 4, pp. 558–567, 2001.
[35] R. S. Yang, A. J. Hanson, B. A. Reese, C. R. Sullivan, and D. J. Perreault, "A low-loss inductor structure and design guidelines for high-frequency applications," *IEEE Transactions on Power Electronics*, vol. 34, no. 10, pp. 9993–10 005, 2019.
[36] W. Liang, L. Raymond, and J. Rivas, "3-d-printed air-core inductors for high-frequency power converters," *IEEE Transactions on Power Electronics*, vol. 31, no. 1, pp. 52–64, 2016.